Static Electronic Density Response of Warm Dense Hydrogen: *Ab Initio* Path Integral Monte Carlo Simulations

Maximilian Böhme[1,2,3] Zhandos A. Moldabekov[1,2] Jan Vorberger[2] and Tobias Dornheim[1,2,*]

[1]*Center for Advanced Systems Understanding (CASUS), D-02826 Görlitz, Germany*
[2]*Helmholtz-Zentrum Dresden-Rossendorf (HZDR), D-01328 Dresden, Germany*
[3]*Technische Universität Dresden, D-01062 Dresden, Germany*

The properties of hydrogen under extreme conditions are important for many applications, including inertial confinement fusion and astrophysical models. A key quantity is given by the electronic density response to an external perturbation, which is probed in x-ray Thomson scattering experiments—the state of the art diagnostics from which system parameters like the free electron density n_e, the electronic temperature T_e, and the charge state Z can be inferred. In this work, we present highly accurate path integral Monte Carlo results for the static electronic density response of hydrogen. We obtain the static exchange-correlation (XC) kernel K_{XC}, which is of central relevance for many applications, such as time-dependent density functional theory. This gives us a first unbiased look into the electronic density response of hydrogen in the warm-dense matter regime, thereby opening up a gamut of avenues for future research.

Matter at extreme densities ($n \sim 10^{21-27}/\text{cm}^3$) and temperatures ($T \sim 10^{4-8}$ K) is ubiquitous throughout our Universe [1]. This so-called warm dense matter [2] (WDM) naturally occurs in a number of astrophysical objects such as giant planet interiors [3,4], brown dwarfs [5], and the outer layers of neutron stars [6,7]. In addition, WDM is highly important for technological applications such as the discovery of novel materials [8,9] and hot-electron chemistry [10]. Moreover, a hydrogen fuel capsule has to traverse the WDM regime [11] on its compression path toward inertial confinement fusion [12]. Consequently, WDM is a highly active research area and a strongly increasing number of experiments [13] are performed at large research facilities such as the National Ignition Facility (NIF) [14], the European X-Ray Free-Electron Laser Facility (XFEL) [15], or the Sandia Z machine [16]. These developments have led to a number of spectacular recent discoveries, including the high-precision measurement of the stopping power in WDM [17], the use of record peak-brightness free-electron lasers to study shock compressed aluminium [18], and the possible observation of the molecular-to-metallic transition in hydrogen at extreme pressure [19,20].

At the same time, we stress that the interpretation of such experiments decisively depends on a rigorous theoretical modeling. In fact, even basic system parameters like the density or electronic temperature are generally unknown and have to be inferred. In this regard, the *x*-ray Thomson scattering (XRTS) technique [21,22] has emerged as the most promising method of diagnostics of WDM experiments.

Unfortunately, the theoretical description of WDM constitutes a most formidable challenge due to the highly nontrivial interplay of a number of physical effects [2,23,24]. WDM states are correlated due to the Coulomb interaction, the electrons (and sometimes the nuclei) are partially quantum degenerate, and WDM is a highly excited state, which rules out the well-stocked arsenal of ground-state quantum many-body methods [25,26]. This intricacy is usually expressed in terms of two characteristic parameters, that are both of the order of unity [27]: (a) the density parameter $r_s = \bar{r}/a_B$, where $\bar{r}$ and a_B are the Wigner-Seitz radius and Bohr radius, and (b) the degeneracy temperature $\theta = k_B T/E_F$, with E_F being the Fermi energy [28].

In this situation, thermal density functional theory (DFT) [29] has emerged as the work horse in WDM theory [2], as it often combines a manageable computation cost with a reasonable degree of accuracy. Yet, the results can substantially depend on the employed exchange-correlation (XC) functional [30], which cannot be obtained within DFT itself, and has to be supplied as a semiempirical *a priori* input; see Ref. [31] for a critical discussion focusing on hydrogen.

An additional challenge pertaining to the interpretation of XRTS experiments is the wave-number dependence of the measured signal. The *ab initio* estimation [32] of the corresponding dynamic structure factor $S(\mathbf{q}, \omega)$ (beyond model assumptions such as the Chihara decomposition [33,34]) requires one to carry out, e.g., linear-response time-dependent DFT (TD DFT) simulations [35], which
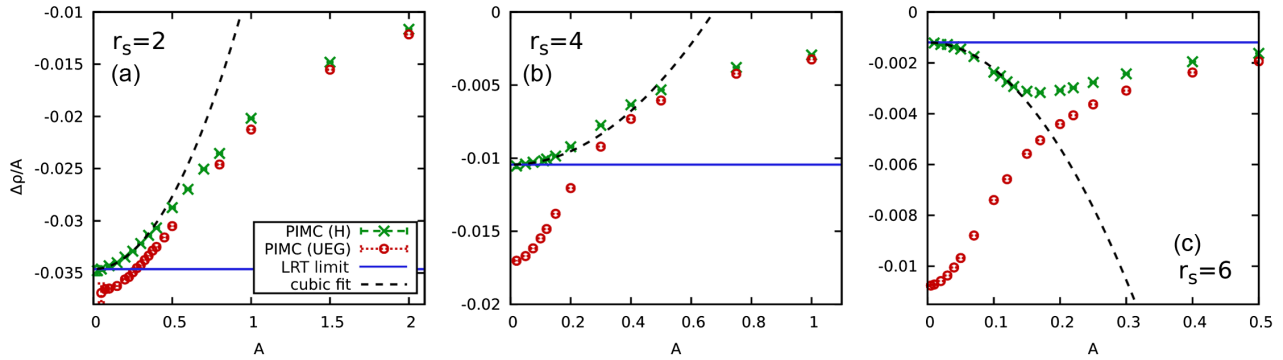
FIG. 1.   Perturbation strength dependence of the electronic density response of hydrogen at $\mathbf{q} = 2\pi L^{-1}(0,0,2)^T$ ($q \approx 1.5q_F$) at the electronic Fermi temperature ($\theta = 1$) for (a) $r_s = 2$, (b) $r_s = 4$, and (c) $r_s = 6$. The green crosses show our new PIMC data for hydrogen, and the red circles corresponding results for a uniform electron gas partly taken from Ref. [40]; note that the statistical error bars do not exceed the symbol size. The dashed black line shows a cubic fit to the PIMC data for $\Delta\rho(A)$, and the solid blue horizontal lines the linear-response limit.

need as input the frequency- and wave-vector-dependent XC kernel $K_{\mathrm{XC}}(\mathbf{q}, \omega)$. Yet, little is known about the actual $K_{\mathrm{XC}}(\mathbf{q}, \omega)$ of a real WDM system, and previous studies [33,36] have been exclusively based on drastic simplifications such as the adiabatic local density approximation (ALDA). This is highly problematic, since these approximate kernels have been designed for the application at $T = 0$ and, in the case of ALDA, are valid only for small wave numbers $q = |\mathbf{q}|$ and break down for strong degrees of inhomogeneity [37].

In the present work, we aim to overcome these limitations for warm dense hydrogen by performing *ab initio* path integral Monte Carlo (PIMC) calculations [38,39] for its static electronic density response. This allows us to thoroughly address a number of fundamental questions, including (i) the quantification of the impact of electron-ion correlations on electronic properties, (ii) the assessment of the validity range of linear response theory and the importance of nonlinear effects [40–42], and (iii) to check widespread model assumptions about the decomposition into *bound* and *free* electrons [22]. Most notably, we present the first, highly accurate results for the XC kernel of a realistic WDM system in the static limit (i.e., $\omega \to 0$). Our theoretical predictions are directly useful for upcoming experiments with hydrogen, for example at NIF or the European XFEL.

Results.—We have carried out thermal DFT–molecular dynamics simulations to obtain a set of ion configurations, and use the PIMC method to obtain exact solutions to the electronic problem in the external ion potential. This allows us to directly compare our PIMC results to DFT, and use the former as input for the latter. We note that we impose no nodal restrictions on the thermal density matrix [43]. Therefore, our PIMC simulations are without approximation, but computationally expensive due to the notorious fermion sign problem [44,45]. We estimate the full computation cost of the present study to be of the order of $\mathcal{O}(10^7)$ CPU hours. To compute the electronic density response, we apply an external harmonic perturbation

[40,46–48] of wave vector $\mathbf{q}$ and perturbation amplitude A, which leads to the full electronic Hamiltonian (we assume Hartree atomic units throughout this work)

$$\hat{H} = -\frac{1}{2}\sum_{l=1}^{N}\nabla_l^2 + \hat{W}_{ee} + \hat{V}_{ei} + 2A\sum_{l=1}^{N}\cos\left(\mathbf{q} \cdot \hat{\mathbf{r}}_l\right). \quad (1)$$

Here, $N = N^\uparrow + N^\downarrow$ is the total number of electrons, and we restrict ourselves to the unpolarized case of $N^\uparrow = N^\downarrow = N/2$. The operators $\hat{W}_{ee}$ and $\hat{V}_{ei}$ denote the interaction between the electrons and the external potential due to the fixed ions, respectively. We use the PIMC method to compute the expectation value of the electronic density in Fourier space $\rho(\mathbf{q}, A) = \langle\hat{\rho}_\mathbf{q}\rangle_{\mathbf{q},A}$, and the sought-after density response is simply given by $\Delta\rho(\mathbf{q}, A) = \rho(\mathbf{q}, A) - \rho(\mathbf{q}, 0)$.

The results for the density response of warm dense hydrogen are shown in Fig. 1 for (a) $r_s = 2$, (b) $r_s = 4$, and (c) $r_s = 6$ at the electronic Fermi temperature, i.e., $\theta = 1$. Specifically, we show $\Delta\rho/A$, and the green crosses (red circles) depict our new PIMC results for hydrogen [for a uniform electron gas (UEG) [40]]; the actual extraction of the linear-response function via cubic fits is discussed below. The main qualitative trends are as follows. For the metallic density of $r_s = 2$, the electrons are only weakly localized around the ions, and the density response both qualitatively and quantitatively resembles the behavior of a UEG at the same conditions. Panel (b) corresponds to a lower electronic density as it is realized experimentally, for example, within hydrogen jets [49]. In this case, a sizable fraction of the electrons is assumed to be involved in *bound states* with the protons. Consequently, we observe a starkly reduced density response compared to the UEG, as only the *unbound* (free) electrons react to the external perturbation; see the discussion of Fig. 2 below. Furthermore, we observe that the data sets for hydrogen and the UEG converge in the limit of large A, since the external perturbation will eventually predominate over the ion potential. Last, Fig. 1(c)
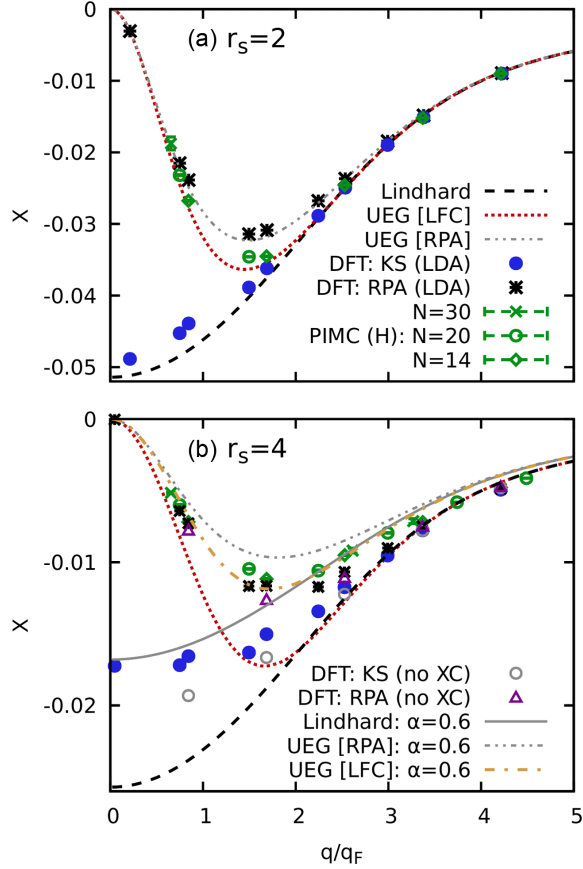
FIG. 2. Electronic density response of warm dense hydrogen at $\theta = 1$ with (a) $r_s = 2$ and (b) $r_s = 4$ (bottom). Green symbols: new PIMC results for different N; blue dots: Kohn-Sham response function within LDA $\chi_0(\mathbf{q})$; black stars: corresponding RPA; dotted red (dash-dotted gray): UEG model with LFC [52] (in RPA); dashed black: Lindhard function. Also shown for $r_s = 4$ are results for the Kohn-Sham response function without XC effects (gray circles), the corresponding RPA (purple triangles), the UEG model assuming a free-electron fraction of $\alpha = 0.6$ (dash-dotted yellow), and the corresponding Lindhard function (solid gray).

shows results for $r_s = 6$. While being hard to probe in current experimental setups, these conditions are interesting as a challenging benchmark for theoretical methods due to the pronounced impact of electronic XC effects [50,51]. In this case, we find that the electronic density response is reduced by an order of magnitude compared to the UEG at small A, due to the high probability of bound states.

An additional advantage of the present approach is its capability to study nonlinear effects and, in this way, to unambiguously assess the validity range of linear response theory. Overall, we find similar trends for hydrogen as in previous investigations of the UEG [40,41], although the manifestation of nonlinear effects is relatively increased in magnitude and changed in sign at $r_s = 6$.

The central task of the present work is the estimation of the linear electronic density response function. The density

response at the first harmonic of the original perturbation (i.e., at the same $\mathbf{q}$) can be expanded in powers of the perturbation amplitude [41] as $\Delta\rho(\mathbf{q}, A) = \chi(\mathbf{q})A + \chi^{\text{cubic}}(\mathbf{q})A^3$, and the dashed black curves depict corresponding fits (see also Ref. [53]) to the PIMC data for sufficiently small A. The horizontal blue lines depict the linear coefficient $\chi(\mathbf{q}) := \chi(\mathbf{q}, 0)$, i.e., the static limit of the linear density response function [71]

$$\chi(\mathbf{q}, \omega) = \frac{\chi_0(\mathbf{q}, \omega)}{1 - \frac{4\pi}{q^2}[1 - G(\mathbf{q}, \omega)]\chi_0(\mathbf{q}, \omega)}. \qquad (2)$$

Here, $\chi_0(\mathbf{q}, \omega)$ can be either the Kohn-Sham response function [53], or the Lindhard function [28] in the case of a uniform system. In addition, $G(\mathbf{q}, \omega) = -(q^2/4\pi) \times K_{\text{XC}}(\mathbf{q}, \omega)$ denotes the local field correction (LFC), which contains the full wave-vector and frequency-resolved information about electronic XC effects, and which is equivalent to the XC kernel K_{XC} usually employed in the context of TD DFT [35]. Both $G(\mathbf{q}, \omega)$ and $K_{\text{XC}}(\mathbf{q}, \omega)$ depend on the particular choice of $\chi_0(\mathbf{q}, \omega)$ and, in the context of DFT, on the employed XC functional.

The relevant linear electronic density response is shown in Fig. 2. The green symbols show our new PIMC results for different N that have been obtained by following the fitting procedure of $\Delta\rho(\mathbf{q}, A)$ outlined above for different wave vectors $\mathbf{q}$. No systematic dependence on the system size (and, therefore, no dependence on individual snapshots) can be resolved, which is consistent to previous findings for the UEG [52,72,73]. We note that $N = 30$ is the maximum possible system size at $r_s = 2$, as it can be seen by the comparably increased error bars in this case. The density response of the UEG has been included as dotted red curves and is in good agreement to the green symbols at $r_s = 2$; we only observe small deviations around $q \sim 1.5q_F$. In stark contrast, there appear pronounced differences between the UEG and hydrogen (exceeding 30%) at $r_s = 4$, which is a direct consequence of the increased location of the electrons around the ions. It is often assumed that the total number of electrons can be decomposed into a *bound* and into an effectively *free* fraction; we denote the latter as $\alpha = N_{\text{free}}/N$ in this work. This leads to the modified parameters $r_s(\alpha) = (3/4\pi n\alpha)^{1/3}$ and $\theta(\alpha) = k_B T / E_F[r_s(\alpha)]$. Empirically, we find that the choice of $\alpha = 0.6$ leads to a good qualitative agreement between the UEG model and our PIMC results for hydrogen at $r_s = 4$ for small to intermediate wave numbers, see the dash-dotted yellow curve in Fig. 2(b). This is close to the result of $\alpha \approx 0.54$ by Militzer and Ceperley [74] based on a cluster analysis in real space. Interestingly, the agreement between the PIMC data for hydrogen and the effective free electron model deteriorates for $q \gtrsim 3q_F$, where the response of hydrogen even slightly exceeds the response of the full UEG model. This is a direct

consequence of the relevant length scale $\lambda = 2\pi/q$ and discussed in detail in Supplemental Material [53].

The blue dots in Fig. 2 depict the Kohn-Sham response function $\chi_0(\mathbf{q})$ that has been computed within the local density approximation (LDA) [75]. For $r_s = 2$, these data closely resemble the Lindhard function [28] (dashed black) describing the uniform ideal Fermi gas. This is expected, as the Kohn-Sham orbitals resemble plane waves when localization is weak. The black stars show the DFT response function within the *random phase approximation*, i.e., by setting $G(\mathbf{q}, 0) = 0$ in Eq. (2). This leads to the correct asymptotes in the limits of large and small q, but becomes inaccurate around $q \sim 1.5q_F$ where electronic XC effects are known to be important [24]. For $r_s = 4$, the Kohn-Sham response function exhibits a more interesting behavior: for large q, it approaches the Lindhard function of the full electronic density, whereas it more closely resembles the reduced Lindhard function corresponding to $\alpha = 0.6$ (solid gray) for $q \lesssim 2q_F$. In other words, some information about electron-ion correlations, in general, and about *bound states*, in particular, is included in the KS response. Remarkably, the corresponding RPA data are in good agreement to the exact PIMC results; more so than for the less strongly coupled case of $r_s = 2$. We also include the KS response function that has been obtained from a DFT simulation without any XC effects for $r_s = 4$ as the gray circles. Interestingly, this leads to substantial differences compared to the blue dots for $q \lesssim 3q_F$, and to a deterioration in the corresponding RPA response function (purple triangles).

Our new PIMC results for the electronic density response of hydrogen give us access to the XC kernel of a realistic WDM system on a true *ab initio* level. The results are shown in Fig. 3 for the same conditions as in Fig. 2. The dotted red curves show results for the full UEG model [52] and the dashed black lines show the ALDA [76,77], which is a parabolic expansion around $q \to 0$. Evidently, the latter is only appropriate for $q < 2q_F$ even in the case of a UEG. Let us next consider the different results that have been obtained from our PIMC results for hydrogen for $\chi(\mathbf{q})$ by inverting Eq. (2) using as input different $\chi_0(\mathbf{q})$. The blue (green) symbols have been obtained using the KS response within LDA (the Lindhard function). At $r_s = 2$, the DFT (LDA-based) kernel agrees qualitatively with the LFC of the UEG. Interestingly, the kernel that has been computed in terms of the Lindhard function exhibits substantial deviations to the other data sets over the entire q range as it has to balance the absence of electron-ion correlations from $\chi_0(\mathbf{q})$, see also Ref. [53].

For $r_s = 4$, the situation is more complicated as none of the data sets computed from $\chi(\mathbf{q})$ resemble the UEG model. For $q \lesssim 2q_F$ [cf. Fig. 2(b)], the LDA-RPA response function is in good agreement with the PIMC results, and the thus extracted LFC is small in magnitude in this regime. This changes for intermediate q, where the LFC becomes comparable in magnitude to the UEG model, but
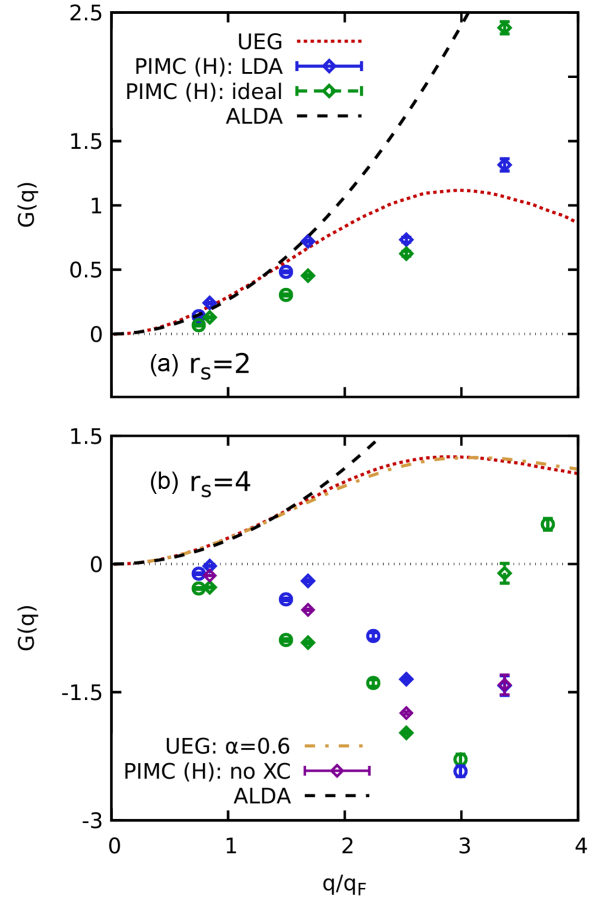

FIG. 3. Electronic local-field correction $G(q) = G(q, 0)$ [cf. Eq. (2)] of warm dense hydrogen for $r_s = 2$ (a) and $r_s = 4$ (b). Dotted red lines: UEG model [52]; blue (green) symbols: solving Eq. (2) for the LFC using for $\chi_0(\mathbf{q})$ the Kohn-Sham response within LDA (the response function of an ideal uniform Fermi gas [78]). The black dashed line gives the ALDA kernel. Also shown are results for the UEG model under the assumption of a free-electron fraction of $\alpha = 0.6$ (dash-dotted yellow) and for the LFC using as input the KS response computed without any XC effects (purple symbols) for $r_s = 4$.

with a negative sign. This is a direct consequence of the overestimation of the actual response by the RPA in the case of hydrogen [cf. Eq. (3) in Ref. [53]], whereas it is well known [52,72] that the opposite holds for the UEG. Using the response function of a uniform ideal Fermi gas to compute the LFC enhances this trend, and the KS response from a DFT simulation with no XC effects is located in between. In addition, this means that using either the ALDA or full UEG model as the XC kernel in a TD DFT calculation of hydrogen leads to an actually worse estimation of the electronic density response compared to the bare RPA at $r_s = 4$.

Conclusion.—In this work, we have presented the first, highly accurate PIMC results for the static electronic density response of hydrogen in the WDM regime. This has allowed us to unambiguously quantify the importance

of nonlinear effects, which are even more important compared to the previously investigated case of a uniform electron gas [40,41,79]. Moreover, we have obtained extensive data for the exact linear-response limit of the static density response function $\chi(\mathbf{q}, 0)$, which have been used to extract the first exact results for the static LFC $G(\mathbf{q})$ and XC kernel $K_{\mathrm{XC}}(\mathbf{q})$. We stress that the latter in general depends on the employed $\chi_0(\mathbf{q}, 0)$, which can be either a Lindhard function or a Kohn-Sham response function that depends on the particular choice of the XC functional. This has profound consequences in the presence of bound states, where the actual XC kernel does not even qualitatively resemble the familiar UEG models. Consequently, the commonly employed ALDA [76,77] is appropriate when most electrons are free and behave similarly to a UEG, but dramatically breaks down when the degree of electronic localization around the protons is substantial; see Supplemental Material [53] for a corresponding TD DFT study.

Our results indicate a strong need for the development and re-evaluation of presently used model XC kernels such as ALDA. A particular advantage of our study is given by the direct possibility to compare our PIMC results for different properties to corresponding DFT results for the same ion configuration. This, in turn, will give us invaluable lessons regarding the performance of different XC functionals [37,80], and guide the development of new approaches [81–85]. Finally, we reiterate the capability of our setup to study *nonlinear effects* in warm dense hydrogen, which may give unprecedented insights into many-body correlation effects in WDM [42] and are known to sensitively depend on important system parameters such as the electronic temperature [86].

---

[*]t.dornheim@hzdr.de

[1] V. E. Fortov, Extreme states of matter on earth and in space, Phys. Usp. **52**, 615 (2009).

[2] *Frontiers and Challenges in Warm Dense Matter*, edited by F. Graziani, M. P. Desjarlais, R. Redmer, and S. B. Trickey (Springer, International Publishing, Cham, 2014).

[3] Alessandra Benuzzi-Mounaix *et al.*, Progress in warm dense matter study with applications to planetology, Phys. Scr. **T161**, 014060 (2014).

[4] B. Militzer, W. B. Hubbard, J. Vorberger, I. Tamblyn, and S. A. Bonev, A massive core in Jupiter predicted from first-principles simulations, Astrophys. J. **688**, L45 (2008).

[5] D. Saumon, W. B. Hubbard, G. Chabrier, and H. M. van Horn, The role of the molecular-metallic transition of hydrogen in the evolution of Jupiter, Saturn, and brown dwarfs, Astrophys. J. **391**, 827 (1992).

[6] E. H. Gudmundsson, C. J. Pethick, and R. I. Epstein, Structure of neutron star envelopes, Astrophys. J. **272**, 286 (1983).

[7] Equilibrium plasma properties. Outer envelopes, in *Neutron Stars 1*, edited by P. Haensel, A. Y. Potekhin, and D. G. Yakovlev (Springer, New York, New York, NY, 2007), pp. 53–114.

[8] D. Kraus *et al.*, Formation of diamonds in laser-compressed hydrocarbons at planetary interior conditions, Nat. Astron. **1**, 606 (2017).

[9] A. Lazicki *et al.*, Metastability of diamond ramp-compressed to 2 terapascals, Nature (London) **589**, 532 (2021).

[10] Mark L. Brongersma, Naomi J. Halas, and Peter Nordlander, Plasmon-induced hot carrier science and technology, Nat. Nanotechnol. **10**, 25 (2015).

[11] S. X. Hu, B. Militzer, V. N. Goncharov, and S. Skupsky, First-principles equation-of-state table of deuterium for inertial confinement fusion applications, Phys. Rev. B **84**, 224109 (2011).

[12] R. Betti and O. A. Hurricane, Inertial-confinement fusion with lasers, Nat. Phys. **12**, 435 (2016).

[13] K. Falk, Experimental methods for warm dense matter research, High Power Laser Sci. Eng. **6**, e59 (2018).

[14] E. I. Moses, R. N. Boyd, B. A. Remington, C. J. Keane, and R. Al-Ayat, The national ignition facility: Ushering in a new age for high energy density science, Phys. Plasmas **16**, 041006 (2009).

[15] Thomas Tschentscher, Christian Bressler, Jan Grünert, Anders Madsen, Adrian P. Mancuso, Michael Meyer, Andreas Scherz, Harald Sinn, and Ulf Zastrau, Photon beam transport and scientific instruments at the european XFEL, Appl. Sci. **7**, 592 (2017).

[16] David Yager-Elorriaga *et al.*, An overview of magneto-inertial fusion on the *z* machine at Sandia National Laboratories, Nucl. Fusion **62**, 042015 (2022).

[17] W. Cayzac *et al.*, Experimental discrimination of ion stopping models near the Bragg peak in highly ionized matter, Nat. Commun. **8**, 15693 (2017).

[18] L. B. Fletcher *et al.*, Ultrabright x-ray laser scattering for dynamic warm dense matter physics, Nat. Photonics **9**, 274 (2015).

[19] M. D. Knudson, M. P. Desjarlais, A. Becker, R. W. Lemke, K. R. Cochrane, M. E. Savage, D. E. Bliss, T. R. Mattsson, and R. Redmer, Direct observation of an abrupt insulator-to-metal transition in dense liquid deuterium, Science **348**, 1455 (2015).

[20] Ranga P. Dias and Isaac F. Silvera, Observation of the Wigner-Huntington transition to metallic hydrogen, Science **355**, 715 (2017).

[21] S. H. Glenzer and R. Redmer, x-ray Thomson scattering in high energy density plasmas, Rev. Mod. Phys. **81**, 1625 (2009).

[22] D. Kraus *et al.*, Characterizing the ionization potential depression in dense carbon plasmas with high-precision

spectrally resolved x-ray scattering, Plasma Phys. Control Fusion **61**, 014015 (2019).

[23] M. Bonitz, T. Dornheim, Zh. A. Moldabekov, S. Zhang, P. Hamann, H. Kählert, A. Filinov, K. Ramakrishna, and J. Vorberger, *Ab initio* simulation of warm dense matter, Phys. Plasmas **27**, 042710 (2020).

[24] T. Dornheim, S. Groth, and M. Bonitz, The uniform electron gas at warm dense matter conditions, Phys. Rep. **744**, 1 (2018).

[25] R. O. Jones, Density functional theory: Its origins, rise to prominence, and future, Rev. Mod. Phys. **87**, 897 (2015).

[26] W. M. C. Foulkes, L. Mitas, R. J. Needs, and G. Rajagopal, Quantum Monte Carlo simulations of solids, Rev. Mod. Phys. **73**, 33 (2001).

[27] Torben Ott, Hauke Thomsen, Jan Willem Abraham, Tobias Dornheim, and Michael Bonitz, Recent progress in the theory and simulation of strongly correlated plasmas: Phase transitions, transport, quantum, and magnetic field effects, Eur. Phys. J. D **72**, 84 (2018).

[28] G. Giuliani and G. Vignale, *Quantum Theory of the Electron Liquid* (Cambridge University Press, Cambridge, England, 2008).

[29] N. David Mermin, Thermal properties of the inhomogeneous electron gas, Phys. Rev. **137**, A1441 (1965).

[30] Kieron Burke, Perspective on density functional theory, J. Chem. Phys. **136**, 150901 (2012).

[31] Carlo Pierleoni, Miguel A. Morales, Giovanni Rillo, Markus Holzmann, and David M. Ceperley, Liquid-liquid phase transition in hydrogen by coupled electron-ion Monte Carlo simulations, Proc. Natl. Acad. Sci. U.S.A. **113**, 4953 (2016).

[32] T. Dornheim, S. Groth, J. Vorberger, and M. Bonitz, *Ab Initio* Path Integral Monte Carlo Results for the Dynamic Structure Factor of Correlated Electrons: From the Electron Liquid to Warm Dense Matter, Phys. Rev. Lett. **121**, 255001 (2018).

[33] A. D. Baczewski, L. Shulenburger, M. P. Desjarlais, S. B. Hansen, and R. J. Magyar, X-Ray Thomson Scattering in Warm Dense Matter without the Chihara Decomposition, Phys. Rev. Lett. **116**, 115004 (2016).

[34] J. Chihara, Difference in x-ray scattering between metallic and non-metallic liquids due to conduction electrons, J. Phys. F **17**, 295 (1987).

[35] C. Ullrich, *Time-Dependent Density-Functional Theory: Concepts and Applications*, Oxford Graduate Texts (Oxford University Press, Oxford, 2012).

[36] Kushal Ramakrishna, Attila Cangi, Tobias Dornheim, Andrew Baczewski, and Jan Vorberger, First-principles modeling of plasmons in aluminum under ambient and extreme conditions, Phys. Rev. B **103**, 125118 (2021).

[37] Zhandos Moldabekov, Tobias Dornheim, Maximilian Böhme, Jan Vorberger, and Attila Cangi, The relevance of electronic perturbations in the warm dense electron gas, J. Chem. Phys. **155**, 124116 (2021).

[38] D. M. Ceperley, Path integrals in the theory of condensed helium, Rev. Mod. Phys. **67**, 279 (1995).

[39] T. Dornheim, S. Groth, A. V. Filinov, and M. Bonitz, Path integral Monte Carlo simulation of degenerate electrons: Permutation-cycle properties, J. Chem. Phys. **151**, 014108 (2019).

[40] Tobias Dornheim, Jan Vorberger, and Michael Bonitz, Nonlinear Electronic Density Response in Warm Dense Matter, Phys. Rev. Lett. **125**, 085001 (2020).

[41] Tobias Dornheim, Maximilian Böhme, Zhandos A. Moldabekov, Jan Vorberger, and Michael Bonitz, Density response of the warm dense electron gas beyond linear response theory: Excitation of harmonics, Phys. Rev. Research **3**, 033231 (2021).

[42] Tobias Dornheim, Jan Vorberger, and Zhandos A. Moldabekov, Nonlinear density response and higher order correlation functions in warm dense matter, J. Phys. Soc. Jpn. **90**, 104002 (2021).

[43] D. M. Ceperley, Fermion nodes, J. Stat. Phys. **63**, 1237 (1991).

[44] M. Troyer and U. J. Wiese, Computational Complexity and Fundamental Limitations to Fermionic Quantum Monte Carlo Simulations, Phys. Rev. Lett. **94**, 170201 (2005).

[45] T. Dornheim, Fermion sign problem in path integral Monte Carlo simulations: Quantum dots, ultracold atoms, and warm dense matter, Phys. Rev. E **100**, 023307 (2019).

[46] S. Moroni, D. M. Ceperley, and G. Senatore, Static Response from Quantum Monte Carlo Calculations, Phys. Rev. Lett. **69**, 1837 (1992).

[47] C. Bowen, G. Sugiyama, and B. J. Alder, Static dielectric response of the electron gas, Phys. Rev. B **50**, 14838 (1994).

[48] T. Dornheim, S. Groth, J. Vorberger, and M. Bonitz, Permutation blocking path integral Monte Carlo approach to the static density response of the warm dense electron gas, Phys. Rev. E **96**, 023203 (2017).

[49] U. Zastrau *et al.*, Resolving Ultrafast Heating of Dense Cryogenic Hydrogen, Phys. Rev. Lett. **112**, 105002 (2014).

[50] S. Mazevet, M. P. Desjarlais, L. A. Collins, J. D. Kress, and N. H. Magee, Simulations of the optical properties of warm dense aluminum, Phys. Rev. E **71**, 016409 (2005).

[51] M. P. Desjarlais, J. D. Kress, and L. A. Collins, Electrical conductivity for warm, dense aluminum plasmas and liquids, Phys. Rev. E **66**, 025401(R) (2002).

[52] T. Dornheim, J. Vorberger, S. Groth, N. Hoffmann, Zh. A. Moldabekov, and M. Bonitz, The static local field correction of the warm dense electron gas: An *ab initio* path integral Monte Carlo study and machine learning representation, J. Chem. Phys. **151**, 194104 (2019).

[53] See Supplemental Material at http://link.aps.org/supplemental/10.1103/PhysRevLett.129.066402 for additional details, which includes Refs. [54–70].

[54] M. F. Herman, E. J. Bruskin, and B. J. Berne, On path integral Monte Carlo simulations, J. Chem. Phys. **76**, 5150 (1982).

[55] A. V. Filinov, V. O. Golubnychiy, M. Bonitz, W. Ebeling, and J. W. Dufty, Temperature-dependent quantum pair potentials and their application to dense partially ionized hydrogen plasmas, Phys. Rev. E **70**, 046411 (2004).

[56] B. Militzer, Computation of the high temperature coulomb density matrix in periodic boundary conditions, Comput. Phys. Commun. **204**, 88 (2016).

[57] Tobias Dornheim, Jan Vorberger, Zhandos A. Moldabekov, and Michael Bonitz, Nonlinear interaction of external perturbations in warm dense matter, Contrib. Plasma Phys. e202100247 (2022).

[58] Aron J. Cohen, Paula Mori-Sánchez, and Weitao Yang, Insights into current limitations of density functional theory, Science **321**, 792 (2008).

[59] Tobias Dornheim, Panagiotis Tolias, Zhandos Moldabekov, Attila Cangi, and Jan Vorberger, Effective electronic forces and potentials from *ab initio* path integral Monte Carlo simulations, J. Chem. Phys. **156**, 244113 (2022).

[60] Yongjun Choi and Michael S. Murillo, Influence of dissipation and effective interaction on the dense plasma dynamic structure factor, Phys. Rev. E **103**, 063210 (2021).

[61] Tobias Dornheim, Zhandos A. Moldabekov, Jan Vorberger, and Burkhard Militzer, Path integral Monte Carlo approach to the structural properties and collective excitations of liquid ^{3}He without fixed nodes, Sci. Rep. **12**, 708 (2022).

[62] M. Thiele, E. K. U. Gross, and S. Kümmel, Adiabatic Approximation in Nonperturbative Time-Dependent Density-Functional Theory, Phys. Rev. Lett. **100**, 153004 (2008).

[63] Stephen L. Adler, Quantum theory of the dielectric constant in real solids, Phys. Rev. **126**, 413 (1962).

[64] Nathan Wiser, Dielectric constant with local field effects included, Phys. Rev. **129**, 62 (1963).

[65] J. J. Mortensen, L. B. Hansen, and K. W. Jacobsen, Real-space grid implementation of the projector augmented wave method, Phys. Rev. B **71**, 035109 (2005).

[66] J. Enkovaara *et al.*, Electronic structure calculations with GPAW: A real-space implementation of the projector augmented-wave method, J. Phys. Condens. Matter **22**, 253202 (2010).

[67] Ask Hjorth Larsen *et al.*, The atomic simulation environment—a PYTHON library for working with atoms, J. Phys. Condens. Matter **29**, 273002 (2017).

[68] S. R. Bahn and K. W. Jacobsen, An object-oriented scripting interface to a legacy electronic structure code, Comput. Sci. Eng. **4**, 56 (2002).

[69] Hendrik J. Monkhorst and James D. Pack, Special points for Brillouin-zone integrations, Phys. Rev. B **13**, 5188 (1976).

[70] T. Dornheim, M. Böhme, and Z. Moldabekov, Data publication: Electronic Density Response of Warm Dense Hydrogen: Ab initio Path Integral Monte Carlo Simulations, 2022, https://rodare.hzdr.de/record/1807.

[71] A. A. Kugler, Theory of the local field correction in an electron gas, J. Stat. Phys. **12**, 35 (1975).

[72] S. Groth, T. Dornheim, and J. Vorberger, *Ab initio* path integral Monte Carlo approach to the static and dynamic density response of the uniform electron gas, Phys. Rev. B **99**, 235122 (2019).

[73] Tobias Dornheim, Travis Sjostrom, Shigenori Tanaka, and Jan Vorberger, Strongly coupled electron liquid: *Ab initio* path integral Monte Carlo simulations and dielectric theories, Phys. Rev. B **101**, 045129 (2020).

[74] B. Militzer and D. M. Ceperley, Path integral Monte Carlo simulation of the low-density hydrogen plasma, Phys. Rev. E **63**, 066404 (2001).

[75] J. P. Perdew and Alex Zunger, Self-interaction correction to density-functional approximations for many-electron systems, Phys. Rev. B **23**, 5048 (1981).

[76] Eberhard K. U. Gross and Neepa T. Maitra, Introduction to TDDFT, in *Fundamentals of Time-Dependent Density Functional Theory*, edited by Miguel A. L. Marques, Neepa T. Maitra, Fernando M. S. Nogueira, E. K. U. Gross, and Angel Rubio (Springer Berlin Heidelberg, Berlin, Heidelberg, 2012), pp. 53–99.

[77] M. J. Stott and E. Zaremba, Linear-response theory within the density-functional formalism: Application to atomic polarizabilities, Phys. Rev. A **21**, 12 (1980).

[78] S. Groth, T. Dornheim, and M. Bonitz, Configuration path integral Monte Carlo approach to the static density response of the warm dense electron gas, J. Chem. Phys. **147**, 164108 (2017).

[79] Tobias Dornheim, Zhandos A. Moldabekov, and Jan Vorberger, Nonlinear density response from imaginary-time correlation functions: *Ab initio* path integral Monte Carlo simulations of the warm dense electron gas, J. Chem. Phys. **155**, 054110 (2021).

[80] Zhandos Moldabekov, Tobias Dornheim, Jan Vorberger, and Attila Cangi, Benchmarking exchange-correlation functionals in the spin-polarized inhomogeneous electron gas under warm dense conditions, Phys. Rev. B **105**, 035134 (2022).

[81] Kushal Ramakrishna, Tobias Dornheim, and Jan Vorberger, Influence of finite temperature exchange-correlation effects in hydrogen, Phys. Rev. B **101**, 195129 (2020).

[82] V. V. Karasiev, L. Calderin, and S. B. Trickey, Importance of finite-temperature exchange correlation for warm dense matter calculations, Phys. Rev. E **93**, 063207 (2016).

[83] S. Groth, T. Dornheim, T. Sjostrom, F. D. Malone, W. M. C. Foulkes, and M. Bonitz, *Ab Initio* Exchange–Correlation Free Energy of the Uniform Electron Gas at Warm Dense Matter Conditions, Phys. Rev. Lett. **119**, 135001 (2017).

[84] Valentin V. Karasiev, Travis Sjostrom, James Dufty, and S. B. Trickey, Accurate Homogeneous Electron Gas Exchange-Correlation Free Energy for Local Spin-Density Calculations, Phys. Rev. Lett. **112**, 076403 (2014).

[85] Valentin V. Karasiev, James W. Dufty, and S. B. Trickey, Nonempirical Semilocal Free-Energy Density Functional for Matter Under Extreme Conditions, Phys. Rev. Lett. **120**, 076401 (2018).

[86] Zhandos A. Moldabekov, Tobias Dornheim, and Attila Cangi, Thermal excitation signals in the inhomogeneous warm dense electron gas, Sci. Rep. **12**, 1093 (2022).